Journal of Innovative Optical Health Sciences
Vol. 4, No. 2 (2011) 191−198

DOI: 10.1142/S1793545811001472

NEAR-INFRARED IMAGING SENSOR WITH IMPROVED HANDLING AND DIRECT LOCALIZATION IN SIMULTANEOUS MAGNETIC RESONANCE IMAGING MEASUREMENTS

SONJA SPICHTIG[*,†,§,‖], MARCO PICCIRELLI[†,‡,¶,‖], ROBERT S. VORBURGER[†] and MARTIN WOLF[*]

[*]*Biomedical Optics Research Laboratory, Division of Neonatology*
University Hospital of Zurich, 8091 Zurich, Switzerland

[†]*Institute for Biomedical Engineering*
University and ETH Zurich, Zurich, Switzerland

[‡]*Laboratory for Social and Neural Systems Research*
Department of Economics, University of Zurich
Zurich, Switzerland

[§]*sonja.spichtig@alumni.ethz.ch*
[¶]*piccirelli@biomed.ee.ethz.ch*

We present a novel optical sensor to acquire simultaneously functional near-infrared imaging (fNIRI) and functional magnetic resonance imaging (fMRI) data with an improved handling and direct localization in the MRI compared to available sensors. Quantitative phantom and interference measurements showed that both methods can be combined without reciprocal adverse effects. The direct localization of the optical sensor on MR images acquired with a T1-weighted echo sequence simplifies the co-registration of NIRI and MRI data. In addition, the optical sensor is simple to attach, which is crucial for measurements on vulnerable subjects. The fNIRI and T2*-weighted fMRI data of a cerebral activation were simultaneously acquired proving the practicability of the setup.

Keywords: Medical optics instrumentation; imaging systems; functional monitoring and imaging.

1. Introduction

Combining different imaging methods ("multi-modal imaging") to enhance the structural and functional understanding of the human body became increasingly interesting during the last 20 years.[1] The functional neuroimaging modality most used is functional magnetic resonance imaging (fMRI). The fMRI indirectly measures the cerebral activity by detecting the blood-oxygen-level-dependent (BOLD) MR signal.[2] Although the application of fMRI is widely used, the mechanism underlying the neurovascular coupling is not yet completely understood.[3,4] Various models have been developed to help understand brain function: from local models for the BOLD-signal (Balloon model)[5] to more sophisticated connectivity models, such as dynamic causal modeling (DCM).[6]

Functional near-infrared imaging (fNIRI) can detect concentration changes not only in deoxyhemoglobin (Δ[HHb]) — the molecule at the basis for the BOLD signal phenomenon — but also in

[‖]These authors contributed equally to this work.

oxy- and total-hemoglobin ($\Delta[O_2Hb]$ and $\Delta[tHb]$).[7,8] The fNIRI data could provide additional information for the models which are used to post-process fMRI data, and might therefore help to understand neurovascular coupling and brain function. In addition, fNIRI benefits from the anatomical MR image, as this can be incorporated as *a priori* information in the process of photon transport modeling to improve the results of the image reconstruction.[9]

Several optical sensors for combined fNIRI–fMRI measurements have been used in the past years. Some of them consist of a single light source combined with a detector,[10,11] whereas others feature multiple light sources and detectors spatially distributed over a part of the head.[12–16] For the latter, the light sources and detectors are either casted in polyurethane, attached to the head with a rather complex Velcro structure or the description is not discussed in methods. Indeed, the majority of the reports omit a detailed description of the single parts used for an optical sensor. But the knowledge of the constituent parts is of crucial importance to avoid any negative side effects when peripherics are introduced into a MR scanner. In addition, phantom measurements should be performed to assess the potential influence of a foreign object on the temporal (e.g., electrostatic discharges in and around the optical sensor) and spatial (e.g., increasing the spatial noise) stability of the MR data. To our knowledge, this aspect has not been discussed in the literature.

MR markers were embedded into most of the optical sensors for co-registration of fNIRI and fMRI data. Attaching individual glass fibers directly to the head has the advantage that the crumpled skin can be located in the MR scan, however, handling of such a sensor is rather complex. Handling becomes a very important issue for measurements on vulnerable patients such as newborn infants, for which a MR scan is indicated and a simultaneously performed NIRI scan would provide additional information about their brain functions. Such studies in this population are important as the hemodynamic response and effective connectivity of the developing brain is thought to be quite different.[17,18]

The aims of the study were (i) to construct a NIRI sensor to enable simultaneous fNIRI–fMRI measurements with an improved handling and direct localization in the MRI, (ii) to detect with qualitative and quantitative tests the potential adverse effects of the NIRI sensor on the MR scanner, (iii) to test the inertness of the NIRI setup to the MR instrumentation, and (iv) to prove the practicability of the setup with a functional measurement of an adult subject.

2. Methods and Materials

2.1. *NIRI instrument and sensor*

The ISS OxiplexTS™ (ISS Inc., Champaign, Illinois, USA) was specifically adapted to enhance its range of applications.[19] Modifications to hardware and software quadrupled the number of detector and light source combinations for a single optical sensor to 16. This increased the probed tissue volume and the spatial resolution of the optical sensor. The time resolution of the novel configuration is 25 Hz compared to 50 Hz for the commercial configuration.

The aim was to build an NIRI sensor without any active and ferrous parts and to use glass fibers connecting the sensor to the NIRI instrument, which are long enough to be able to place the instrument itself outside the MR scanner room.

The optical sensor was constructed using the following parts: 10-m long glass fibers for the source fibers (BFL37-400, Thorlabs, Newton, NJ, USA), 10-m long glass fibers for the detector fibers (LP3, Fiberoptic-Heim, Bühler, Switzerland), prisms (Balboa Scientific, Costa Mesa, CA, USA), plastic ferrules and an epoxy (EPO-TEK® 302, Epoxy Technology Inc., Billerica, MA, USA) to fix one end of two fibers (690 and 830 nm) in a plastic ferrule and to attach it in a further step to the prisms. A medical grade silicone elastomer (Silpuran 6000/10, Wacker Silicone, Munchen, Germany) was used to cast the fibers in it and different black colors to dye the silicone elastomer (Table 1). The color to dye the silicone was chosen based on the results of dyed

Table 1. Dyes used to produce the silicone pads.

Name	Dye
A1	Carbon black powder (CB)[a]
A2	Pigment paste FL dark black[b]
A3	Pigment paste FI205[c]
A4	ELASTOSIL® pigment paste PT 9005[d]
A5	CB[a], ELASTOSIL® pigment paste PT 9005[d]

[a]Alfa Aesar, Ward Hill, MA, USA.
[b]R&G GmbH, Waldenbuch, Germany.
[c]Factor II, Lakeside, AZ, USA.
[d]Wacker Silicone, Munich, Germany.

silicone pads in the MR scanner (Secs. 2.2 and 3.1). Finally, connectors (10410A, Thorlabs Newton, Newton, NJ, USA) were attached at the other end of the fibers to connect the source fibers with the ISS OxiplexTS^{TM}.

2.2. *Measurements of dyed silicone pads*

Different colors (Table 1) were mixed with the silicone elastomer to produce dyed silicone pads of approximately the size and thickness of the planned optical sensor. The pads were tested for the artifacts induced on MR data and the possibility to localize them in the MRI.

For the measurements, the dyed silicone pads were affixed on a spherical water phantom (Sphere A water phantom, Philips Healthcare, Best, The Netherlands) with elastic bandages and placed in the center of the head coil (SENSE 8-Channel Headcoil, Philips Healthcare, Best, The Netherlands). The phantom was positioned close to the center of the coil with foam pads and secured with foam wedges. A sandbag was placed on the top of the coil.

Two MR sequences were applied: firstly, a modified BIRN sequence,[20] which is a gradient-echo BOLD fMRI T2*-weighted sequence very sensitive to susceptibility artifacts due to the large echo planar imaging (EPI) factor (79) and the fast readout gradients (slew rate 200 mT/m/ms, max. amplitude 28 mT/m); and secondly, a T1-weighted Turbo Field Echo (TFE) sequence. At this stage, a qualitative comparison of the dyed silicone pads data was sufficient, as will appear evident in Sec. 3.

2.3. *Quantitative phantom measurements*

2.3.1. *MRI signal stability*

Due to the small amplitude of the BOLD signal, a stable performance of the MR scanner is required for fMRI. To assess if the NIRI sensor influences the spatial and temporal stability of the MR scanner, quantitative phantom measurements were performed and analyzed according to Ref. 20. Twelve sequences of 200 images were acquired of the sole spherical water phantom and afterward with the NIRI sensor attached to it. Mean and standard deviation (STD) were calculated for the signal-to-noise ratio (SNR), the signal to (temporal) fluctuation noise ratio (SFNR), the relative STD for single pixels, the noise spectrum peak, the drift, the ghost intensity, the relative STD for the largest region of interest (ROI), and the radius of decorrelation.[20] To assess if the temporal and spatial stability of the MR scanner is influenced by the optical sensor, a two-sided t-test ($\alpha < 0.05$) was performed with the H_0 hypothesis that the above-mentioned parameters are not influenced by the NIRI sensor.

2.3.2. *Evaluation of the NIRI inertness*

To evaluate the effects of the rf-pulses and magnetic field gradients applied during functional MR scans on the NIRI instruments, the NIRI sensor was attached to an optical silicone phantom and placed under the spherical water phantom in the head coil. Foam pads and foam wedges were used to place and secure both phantoms. For the measurements, 50 stimulation blocks were applied for 2 s when the MRI acquisition was on (t_{ON}) and 2 s when they were off (t_{OFF}). The $\Delta[O_2Hb]$ and $\Delta[HHb]$ values were calculated using the modified Lambert−Beer law[21] and averaged for each stimulation block (x_{ON}) over t_{ON} and (x_{OFF}) over t_{OFF}. The means were compared pairwise with a two-sided t-test ($\alpha < 0.05$) for each single light path. The H_0 hypothesis was that the NIRI signal is not influenced by the MRI acquisition.

2.4. *Functional measurements*

For the functional measurements with simultaneous NIRI−MRI recording, a finger-tapping paradigm was chosen. A 16-s rest was followed by 16 s tapping and applied 13 times. The software Presentation (Neurobehavioral Systems Inc., Albany, CA, USA) was used to generate an auditory signal to indicate each single tapping event for the subject. The time between two tapping events was varied between 475 to 525 ms. The computer running Presentation, the MR scanner and the ISS OxiplexTS^{TM} were time synchronized by an analog trigger signal issued by the MR scanner.

To determine the subject-specific localization of the motor cortex, the finger-tapping paradigm was once carried out before the attachment of the optical sensor. This allowed a positioning of the optical sensor over the targeted cortex area. Afterward, an anatomical head scan was acquired using a T1-weighted TFE sequence. For the functional

measurement, a multi-slice gradient-echo T2*-weighted BOLD fMRI sequence with fast encoding gradients (slew rate 200 mT/m/ms, max. amplitude 21 mT/m) and an EPI factor of 65 was applied. The sequence used for the functional measurements is an extreme case; conventional fMRI sequences are less sensitive to magnetic field perturbations.

The BOLD signal was analyzed online with Iview Bold (Philips Healthcare, Best, The Netherlands) using a *minimal cluster size* of 9 pixels, a *threshold value* of 5% and a noise discard level *mask* of 79 arbitrary units. The fMRI data and the statistical map were exported for offline analysis. The fMRI signal of the brain voxel with the highest *t*-value was averaged with its 26 nearest neighbors. This averaged signal was Fourier transformed and the frequencies' below 0.02 Hz and above 0.2 Hz were deleted before back Fourier transformation. Finally, the signal average and STD over these 13 samples were calculated.

For the fNIRI analysis, $\Delta[O_2Hb]$, Δ[HHb] and Δ[tHb] were calculated from the optical intensity data using the modified Lambert−Beer law.[21] The differential path length factors (DPF) given in the literature[22] for C3 at 759 and 834 nm were linearly interpolated to find: $DPF_{690\,nm} = 8.21$ and $DPF_{830\,nm} = 7.3$. Concentration time series were band-pass filtered (0.02−0.2 Hz). A mean was calculated for each 2 s to obtain the same sampling rate as the fMRI data and to enable a direct temporal comparison. Over a stimulation block, the mean was subtracted according to the fMRI analysis. For each light path, the signal average and STD over the 13 stimulation blocks were calculated and the light path showing the most prominent stimulus response was chosen for the fMRI comparison.

3. Results

3.1. *Measurements of dyed silicone pads*

The acquired images of the silicone pads attached to the water phantom are shown in Fig. 1. The silicone pads A2 and A3 produced significant artifacts in the images, probably due to iron particles present in the dye. The CB and the ELASTOSIL® pigment paste PT 9005 did not produce artifacts and are thus suitable for usage in the MR scanner. We decided to dye the main body of the NIRI sensor with CB and the contact surface (with a thickness of around 1 mm) with ELASTOSIL® pigment paste PT 9005.

3.2. *Quantitative phantom measurements*

3.2.1. *MRI signal stability*

All parameters for the MRI signal stability analysis are listed in Table 2 with *p*-value. No significant differences were found for any parameter suggesting that introducing the NIRI sensor into the MR scanner does not significantly influence the scanners' performance.

3.2.2. *Evaluation of the degree of inertness of the fNIRI setup*

No significant concentration differences between x_{ON} and x_{OFF} were found. The maximum difference of a light path was 0.023 μM for $[O_2Hb]$ ($p = 0.184$) and 0.005 μM for [HHb] ($p = 0.113$). These values are much smaller (15 to 50 times) than the concentration changes elicited by a functional activation, implying

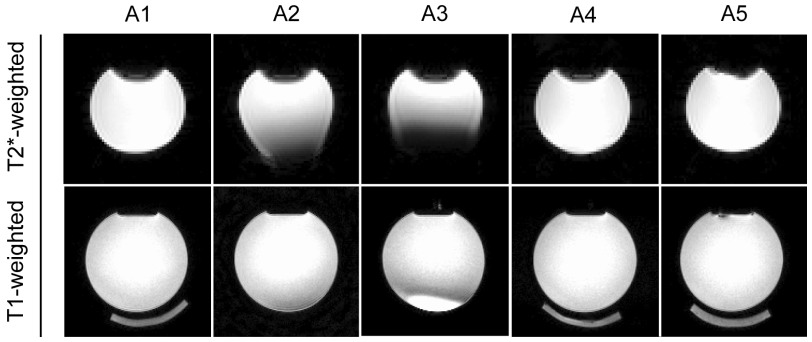

Fig. 1. The MR images of different silicone pads attached underneath a spherical water phantom were acquired with a gradient-echo BOLD fMRI T2*-weighted and TFE T1-weighted sequences. The elliptical artifacts on top originated from the air−water interface inside the phantom. The silicone pads are visible in the T1-weighted images for the pads A1, A4, and A5.

Table 2. Comparison of the mean and STD of the water phantom with and without the NIRI sensor attached to it.

	Sole water phantom		NIRI sensor attached		Comparison
Parameter	Mean	STD	Mean	STD	p-value
Relative STD single pixel	0.363	0.045	0.356	0.049	0.73
Relative STD largest ROI	0.225	0.054	0.221	0.061	0.85
RDC	1.65	0.20	1.66	0.21	0.92
Drift	0.076	0.309	0.074	0.173	0.99
SNR summary value	369	28	371	21	0.93
SFNR summary value	288	27	291	32	0.75
Noise spectrum peak	8.05	2.40	7.81	2.83	0.83
Ghost	1.50	0.53	1.53	0.61	0.90

All parameters of the MRI signal stability analysis are listed.

that these differences are within random fluctuations. This shows that fMRI acquisition has no significant adverse effects on the NIRI setup.

3.3. *Functional measurements*

The dataset of the anatomical head scan was imported to MRIcro software.[23] The temporal evolution of the average hemodynamic responses measured by fNIRI and fMRI are shown in Fig. 2. The BOLD signal was scaled to enable a direct comparison of the fNIRI and fMRI signal. No response to the stimulus was detected for Δ[HHb], whereas the Δ[O_2Hb] and BOLD signal showed a simultaneous increase after the stimulus onset. A 3D head model was generated with the surface render function of MRIcro software and the NIRI sensor was clearly visible (Fig. 3). In the fNIRI, the signal was localized, i.e., a significant change in Δ[O_2Hb] was found in 6 of 16 light paths, i.e., the signal cannot be due to a systemic and superficial response, which would affect all paths in the same way. The localization of the BOLD and fNIRI response were compared, taking advantage of the good visibility of the NIRI sensor. A good agreement was found, as the light paths showing a response were indeed located on the head surface above the BOLD response.

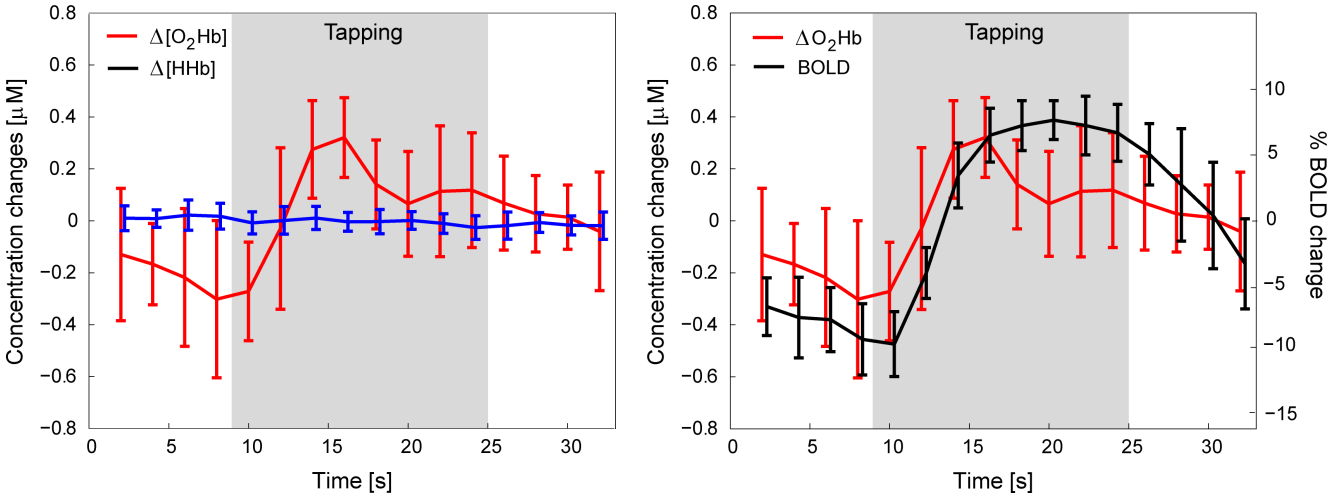

(a) (b)

Fig. 2. Temporal evolution of the stimulus response for Δ[O_2Hb] and Δ[HHb] (left panel) and the comparison of Δ[O_2Hb] with the scaled BOLD response (right panel). The signal average and STD (shown with the error bars) were calculated over the 13 stimulus repetitions.

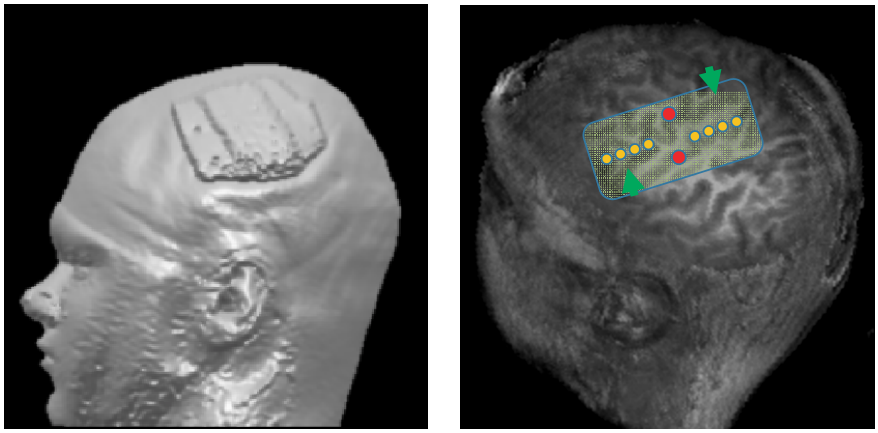

(a) (b)

Fig. 3. Surface-rendered anatomical head scan shows subject's head with attached NIRI sensor (left). Schematic of the position of the sensor on the head (right). The larger red circles represent the detectors, the yellow small circles represent light sources. All combinations of the paths between light sources and detectors were measured. The arrows point to the sulcus. The motor sulcus is parallel to the light sources.

4. Discussion

To the best of our knowledge, the important aspects of tests to exclude reciprocal adverse effects between the NIRI sensor and the MR scanner have not yet been discussed in the literature. In addition, most of the available sensors are complicated to handle and hence their use is restricted to healthy and stable subjects.

The advantages of the presented NIRI sensor are: (i) that there are no reciprocal adverse effects between the NIRI sensor and the MR scanner, (ii) the localization of the NIRI sensor on the MR image, which will simplify co-registration of both methods, (iii) the influence of the dielectric coating of the optical prisms on the MR images is negligible, and (iv) the NIRI sensor is simple to handle.

The practicability of the combined NIRI−MRI setup was shown with functional measurements. A simultaneous increase in [O_2Hb] and the BOLD signal was observed, however, no [HHb] response was seen. This unexpected [HHb] course could result from a low signal-to-noise ratio as NIRI is in general more sensitive to [O_2Hb] changes than to [HHb] changes. The high inertness of the imaging systems to each other was achieved by using purely passive optical components and iron-free parts. The visibility of the silicone elastomer in the MR image is caused by the H-atoms in the organic side groups attached to the Si atoms.

One limitation of the presented NIRI sensor is that it covers only part of the head due to its limited size. This implies that the sensor needs to be placed on the head surface located above the cerebral activation. But since the hemodynamic response to a specific stimulus is localized, localized measurements are sufficient to improve the hemodynamic models.

This thoroughly tested NIRI sensor provides an excellent tool to study local brain function in order to understand the physiology of the neurovascular coupling and to improve hemodynamic models. Considering the approach presented by Sassaroli *et al.*,[14] i.e., multiplying the spatial BOLD signal with the conditional probability that a detected photon passes through a specific voxel, the volume probed by NIRS gets considered in the analysis and the correlation between the fNIRI and the BOLD signal should increase. In addition, the anatomical MR image can be incorporated to the photon transport model to improve image reconstruction from NIRI data.

To summarize, this is the first report of a NIRI sensor being visible on T1-weighted MR images and of a thorough setup testing to exclude negative side effects due to potential interferences between imaging methods. The simple handling of the NIRI sensor and thus the minimal disturbance of the subject makes it a promising tool for multimodal imaging investigations of vulnerable subjects, such as newborn infants.

Acknowledgments

The authors gratefully acknowledge the support of the Swiss National Foundation (National Research

Programme NRP 57) and like to thank Andreas Metz for his dedication. We thank Klaas Enno Stephan for supporting this study and Philips Healthcare for technical and financial support. We like to address special thanks to Elisabeth Moore from Philips Healthcare for providing and answering questions about the MRI stability test post-processing software, to Dennis Hueber from ISS Inc. for answering questions about the ISS OxiplexTS^{TM} and to Cornelia Hagmann for proof-reading the manuscript.

References

1. P. Cerretelli, T. Binzoni, "The contribution of NMR, NIRS and their combination to the functional assessment of human muscle," *Int. J. Sports Med.* **18**(Suppl 4), S270−S279 (1997).
2. S. Ogawa, T. M. Lee, A. S. Nayak, P. Glynn, "Oxygenation-sensitive contrast in magnetic resonance image of rodent brain at high magnetic fields," *Magn. Reson. Med.* **14**(1), 68−78 (1990).
3. N. K. Logothetis, J. Pauls, M. Augath, T. Trinath, A. Oeltermann, "Neurophysiological investigation of the basis of the fMRI signal," *Nature* **412**(6843), 150−157 (2001).
4. N. K. Logothetis, "What we can do and what we cannot do with fMRI," *Nature* **453**(7197), 869−878 (2008).
5. R. B. Buxton, E. C. Wong, L. R. Frank, "Dynamics of blood flow and oxygenation changes during brain activation: The balloon model," *Magn. Reson. Med.* **39**(6), 855−864 (1998).
6. K. J. Friston, L. Harrison, W. Penny, "Dynamic causal modelling," *Neuroimage* **19**(4), 1273−1302 (2003).
7. M. Wolf, M. Ferrari, V. Quaresima, "Progress of near-infrared spectroscopy and topography for brain and muscle clinical applications," *J. Biomed. Opt.* **12**(6), 062104 (2007).
8. M. Wolf, U. Wolf, V. Toronov, A. Michalos, L. A. Paunescu, J. H. Choi, E. Gratton, "Different time evolution of oxyhemoglobin and deoxyhemoglobin concentration changes in the visual and motor cortices during functional stimulation: A near-infrared spectroscopy study," *Neuroimage* **16**(3 Pt 1), 704−712 (2002).
9. M. Schweiger, S. R. Arridge, "Optical tomographic reconstruction in a complex head model using *a priori* region boundary information," *Phys. Med. Biol.* **44**(11), 2703−2721 (1999).
10. D. J. Mehagnoul-Schipper, B. F. van der Kallen, W. N. Colier, M. C. van der Sluijs, L. J. van Erning, H. O. Thijssen, B. Oeseburg, W. H. Hoefnagels, R. W. Jansen, "Simultaneous measurements of cerebral oxygenation changes during brain activation by near-infrared spectroscopy and functional magnetic resonance imaging in healthy young and elderly subjects," *Hum. Brain Mapp.* **16**(1), 14−23 (2002).
11. A. Kleinschmidt, H. Obrig, M. Requardt, K. D. Merboldt, U. Dirnagl, A. Villringer, J. Frahm, "Simultaneous recording of cerebral blood oxygenation changes during human brain activation by magnetic resonance imaging and near-infrared spectroscopy," *J. Cerebr. Blood F. Met.* **16**(5), 817−826 (1996).
12. V. Toronov, A. Webb, J. H. Choi, M. Wolf, A. Michalos, E. Gratton, D. Hueber, "Investigation of human brain hemodynamics by simultaneous near-infrared spectroscopy and functional magnetic resonance imaging," *Med. Phys.* **28**(4), 521−527 (2001).
13. G. Strangman, J. P. Culver, J. H. Thompson, D. A. Boas, "A quantitative comparison of simultaneous BOLD fMRI and NIRS recordings during functional brain activation," *Neuroimage* **17**(2), 719−731 (2002).
14. A. Sassaroli, B. Frederick, Y. Tong, P. F. Renshaw, S. Fantini, "Spatially weighted BOLD signal for comparison of functional magnetic resonance imaging and near-infrared imaging of the brain," *Neuroimage* **33**(2), 505−514 (2006).
15. T. J. Huppert, R. D. Hoge, S. G. Diamond, M. A. Franceschini, D. A. Boas, "A temporal comparison of BOLD, ASL, and NIRS hemodynamic responses to motor stimuli in adult humans," *Neuroimage* **29**(2), 368−382 (2006).
16. H. Toyoda, K. Kashikura, T. Okada, S. Nakashita, M. Honda, Y. Yonekura, H. Kawaguchi, A. Maki, N. Sadato, "Source of nonlinearity of the BOLD response revealed by simultaneous fMRI and NIRS," *Neuroimage* **39**(3), 997−1013 (2008).
17. K. Kotilahti, I. Nissila, M. Huotilainen, R. Makela, N. Gavrielides, T. Noponen, P. Bjorkman, V. Fellman, T. Katila, "Bilateral hemodynamic responses to auditory stimulation in newborn infants," *Neuroreport* **16**(12), 1373−1377 (2005).
18. T. Nishida, T. Kusaka, K. Isobe, S. Ijichi, K. Okubo, T. Iwase, K. Kawada, M. Namba, T. Imai, S. Itoh, "Extrauterine environment affects the cortical responses to verbal stimulation in preterm infants," *Neurosci. Lett.* **443**(1), 23−26 (2008).
19. S. Spichtig, *Multi-Distance and Multi-Frequency Frequency-Domain Near-Infrared Imaging: Characterization and Application*, Ph.D. thesis, ETH Zurich, Zurich (2010).
20. L. Friedman, G. H. Glover, "Report on a multicenter fMRI quality assurance protocol," *J. Magn. Reson. Imaging* **23**(6), 827−839 (2006).

21. S. J. Matcher, C. E. Elwell, C. E. Cooper, M. Cope, D. T. Delpy, "Performance comparison of several published tissue near-infrared spectroscopy algorithms," *Anal. Biochem.* **227**(1), 54−68 (1995).
22. H. Zhao, Y. Tanikawa, F. Gao, Y. Onodera, A. Sassaroli, K. Tanaka, Y. Yamada, "Maps of optical differential pathlength factor of human adult forehead, somatosensory motor and occipital regions at multi-wavelengths in NIR," *Phys. Med. Biol.* **47**(12), 2075−2093 (2002).
23. C. Rorden, "MRIcro," http://www.mricro.com.